Atomization and Sprays, 23 (1): 71–95 (2013)

DIESEL SPRAY CFD SIMULATIONS BASED ON THE Σ-Y EULERIAN ATOMIZATION MODEL†

J. M. García-Oliver,[1] J. M. Pastor,[1,*] A. Pandal,[1] N. Trask,[2] E. Baldwin,[2] & D. P. Schmidt[2]

[1]*CMT-Motores Térmicos, Universitat Politècnica de València, Spain*

[2]*Department of Mechanical and Industrial Engineering, University of Massachusetts, Amherst, Massachusetts, USA*

[*]Address all correspondence to J. M. Pastor E-mail: jopasen@mot.upv.es

Original Manuscript Submitted: 12/02/2013; Final Draft Received: 12/04/2013

This work presents an implementation and evaluation of the Σ-Y atomization model for Diesel spray CFD simulations. The Σ-Y model is based on an Eulerian representation of the spray atomization and dispersion by means of a single-fluid variable density turbulent flow within a RANS framework. The locally homogeneous flow approach has been applied in order to develop a spray vaporization model based on state relationships. A finite-volume solver for model equations has been created using the OpenFOAM CFD open-source C++ library. Model predictions have been compared to experimental data from free Diesel sprays under nonvaporizing and vaporizing conditions. High-speed imaging, PDPA, and Rayleigh-scattering measurements have been used in order to assess the CFD model. Accurate predictions of liquid and vapor spray penetration, as well as axial velocity and mixture fraction profiles, can be simultaneously achieved for a wide range of injection pressure and ambient conditions, despite only having qualitatively correct predictions of droplet size. The success of these predictions supports the mixing-limited vaporization hypothesis. Model accuracy is better for high ambient density and injection pressure conditions. It is proposed that under low ambient density and injection pressure conditions, interfacial dynamics become more important and the single velocity field assumption is less appropriate.

KEY WORDS: *Eulerian, Diesel, evaporation, CFD*

1. INTRODUCTION

The fuel injection process and subsequent fuel-air mixing formation play a major role in combustion and pollutant formation in Diesel engines. Therefore, an accurate prediction of these processes is required in order to produce reliable engine performance and emissions predictions. Diesel spray modeling is still a challenging task due to the complex interrelated phenomena involved; some of them, such as primary atomization

†Part of this work was presented at the ICLASS 2012 Conference in Heidelberg, Germany, September 2–6, 2012.

1044–5110/13/$35.00

NOMENCLATURE

A	surface-area production rate
a	surface-area production rate
a_{coll}	surface-area production rate from collision
a_p	diagonal coefficient from momentum equation
C_ϵ	modeling constant for turbulence closure
D	nozzle orifice outlet diameter
D_{32}	local Sauter mean diameter
D_Σ	suitable diffusion coefficient
h	enthalpy
h_f	enthalpy of formation
k	turbulent kinetic energy
K_r	density relaxation constant
L	nozzle orifice length
$\dot{m}$	mass flow rate
p	pressure
r	nozzle orifice inlet radius
r_{eq}	predicted equilibrium droplet radius
R_g	gas constant
Sc	Schmidt number
u	velocity
V_s	coalescence interface destruction coefficient
Y	liquid fraction
Z	mixture fraction

Greek Symbols

α	modeling constant
ϵ	turbulent dissipation rate
μ	viscosity
Σ	mean interfacial surface-area density
σ	surface-tension coefficient
ρ	density
τ	time scale
ϕ	flux at cell faces
Ψ	compressibility

Superscripts

$\bar{}$	volume-averaged quantity
$\tilde{}$	Favre-averaged quantity
$'$	fluctuating quantity

Subscripts

g	gas quantity
l	liquid quantity

(Gorokhovski and Herrmann, 2008) or nozzle cavitation (Schmidt and Corradini, 2001), are not fully understood.

The discrete droplet method (DDM) (Dukowicz, 1980) has been widely employed for Diesel spray modeling on practical design applications for more than 30 years. This method applies a Lagrangian description of the liquid spray, which presents some well known drawbacks for dense two-phase flow modeling. Some basic hypotheses, such as low liquid volume fraction or homogeneously distributed parcels in the computational cells, are not valid in the near nozzle flow of Diesel sprays. In order to assure numerical stability, it is often necessary to use grid sizes larger than the orifice diameter resulting in inadequately resolved flow structures (Abraham, 1997; Iyer and Abraham, 1997). Moreover, the validity of isolated drop based models in this region that is characterized by strong interaction between phases is hardly justified. These issues usually require a

"best-practice" approach when using this method (Abraham and Picket, 2010; Som and Aggarwal, 2009).

The DDM method emphasizes droplet dynamics, with considerable effort devoted to faithfully representing breakup and collision processes. However, at the high ambient pressures present in Diesel engines, turbulent mixing may be the dominant phenomenon. For example, reduced-order models and detailed experimental measurements by Siebers (1998, 1999, 2008) show that characteristic vaporization lengths can be predicted by means of mixing-controlled assumptions, which concludes that individual droplet dynamics are of little significance. His results indicate that "the processes of atomization and the ensuing interphase transport of mass and energy at droplet surfaces are not limiting steps with respect to fuel vaporization in DI diesel sprays." Instead, his experimental measurements and corresponding models indicate that turbulent spray mixing and gas entrainment are pivotal.

A potentially better modeling paradigm would emphasize turbulent mixing and maintain close coupling between the two phases. The Σ-Y atomization model, initially proposed by Vallet and Borghi (1999), has emerged as an alternative to the DDM for Diesel spray simulations (Desportes et al., 2010; Lebas et al., 2005, 2009). This model is based on an Eulerian approach which is more suitable for the description of the primary atomization occurring in the near field of Diesel sprays. Implementations that include a transition to the Lagrangian particle tracking in the sparse downstream spray are referred to as Eulerian-Lagrangian spray atomization (ELSA) (Blokkeel et al., 2003). In the Eulerian model, the extent of the atomization process is computed from an interface surface density equation, and then it is not required to presume any particular shape for liquid fragments. Furthermore, this is a natural approach for including nozzle geometry flow effects on spray calculations (Ning et al., 2009).

In this work, an implementation of the Σ-Y model within the OpenFOAM (Weller et al., 1998) CFD framework is presented. The aim of the paper is to evaluate the application of Σ-Y to Diesel spray modeling by comparing with experimental data. Those data were obtained on specific rigs for spray characterization, including both global and local parameters, such as tip penetration, droplet velocity, and fuel vapor mixture fraction, on a wide range of ambient and injection conditions. Included in this overall objective is the evaluation of the vaporization model, based on mixing-controlled assumptions, and numerical improvements to previous implementation (Trask et al., 2012).

2. MODEL DESCRIPTION

2.1 Modeling Approach

The Σ-Y model treats the liquid/gas mixture as a pseudo-fluid with a single velocity field. Under the assumption that the flow exiting the injector is operating at large Reynolds

and Weber numbers, it is possible to assume a separation of the large-scale flow features, such as mass transport, from the atomization process occurring at smaller scales. This allows the direct simulation of the large-scale bulk transport of the liquid while unresolved turbulent transport is modeled using standard closures such as those used in Reynolds-averaged turbulence models.

To track the dispersion of the liquid phase an indicator function is used taking a value of unity in the liquid phase and zero in the gas phase. The mean liquid volume fraction is denoted ($\overline{Y}$) and the mean mass-averaged fraction is defined as [$\tilde{Y} = (\overline{\rho Y})/\bar{\rho}$]. Favre averaging the transport equation for the liquid mass fraction yields

$$\frac{\partial \bar{\rho}\tilde{Y}}{\partial t} + \frac{\partial \bar{\rho}\tilde{u}_i\tilde{Y}}{\partial x_i} = -\frac{\partial \bar{\rho}\widetilde{u'_i Y'}}{\partial x_i} - \bar{\rho}\tilde{\dot{Y}}_{vap} \tag{1}$$

where u' denotes the density weighted turbulent fluctuations in velocity, Y' denotes turbulent fluctuations in liquid mass fraction and the last term accounts for vaporization, which will be discussed later. The turbulent diffusion liquid flux captures the effect of the relative velocity between the two phases (Vallet et al., 2001). While the approach used here assumes that the resolved momentum of the liquid/gas mixture can be characterized by a single bulk velocity, the slip velocity can be expressed explicitly as derived by Demoulin et al. (2007)

$$u_i|_l - u_i|_g = \frac{1}{\tilde{Y}\left(1-\tilde{Y}\right)} \cdot \widetilde{u'_i Y'} \tag{2}$$

Under the assumption that the two phases form an immiscible mixture, the mass-averaged value of the indicator function is related to the density by

$$\frac{1}{\bar{\rho}} = \frac{\tilde{Y}}{\rho_l} + \frac{1-\tilde{Y}}{\rho_g} \tag{3}$$

An equation of state is then assigned to each phase. The gas phase obeys an ideal gas law, while the liquid phase is assumed to have a linear compressibility, denoted by ψ_l:

$$\rho_g = \frac{p}{R_g T} \tag{4}$$

$$\rho_l = \rho_{l,o} + \psi_l(p - p_o) \tag{5}$$

where $\rho_{l,o}$ and p_o denote reference density and pressures, respectively, about which the equation of state is linearized.

To finally close the above system of equations the temperature is obtained from a bulk mixture enthalpy equation and closures must be given for the terms resulting from Favre averaging. The closure in the liquid mass transport equation is assigned using a standard turbulent gradient flux model,

$$\bar{\rho}\widetilde{u_i'Y'} = \frac{\mu_t}{Sc}\frac{\partial \tilde{Y}}{\partial x_i} \tag{6}$$

and the closure corresponding to the Reynolds stresses in the momentum equation is given by a modified k-ε model,

$$\frac{\partial \bar{\rho}\tilde{k}}{\partial t} + \frac{\partial \bar{\rho}\tilde{u}_i\tilde{k}}{\partial x_i} = \frac{\partial}{\partial x_i}\left(\frac{\mu_t}{P_{rk}}\frac{\partial \tilde{k}}{\partial x_i}\right) - \bar{\rho}R_{ij}\frac{\partial \tilde{u}_j}{\partial x_i} - \overline{u'_i}\frac{\partial \overline{p}}{\partial x_i} - \bar{\rho}\tilde{\varepsilon} \tag{7}$$

$$\frac{\partial \bar{\rho}\tilde{\varepsilon}}{\partial t} + \frac{\partial \bar{\rho}\tilde{u}_i\tilde{\varepsilon}}{\partial x_i} = \frac{\partial}{\partial x_i}\left(\frac{\mu_t}{P_{r\varepsilon}}\frac{\partial \tilde{\varepsilon}}{\partial x_i}\right) + C_{\varepsilon 1}\frac{\tilde{\varepsilon}}{\tilde{k}}\left(-\bar{\rho}R_{ij}\frac{\partial \tilde{u}_j}{\partial x_j} - \overline{u'_i}\frac{\partial \overline{p}}{\partial x_i}\right) - C_{\varepsilon 2}\bar{\rho}\frac{\tilde{\varepsilon}^2}{\tilde{k}} \tag{8}$$

$$-\bar{\rho}\widetilde{u_i'u_j'} = \mu_t\left(\frac{\partial \tilde{u}_i}{\partial x_j} + \frac{\partial \tilde{u}_j}{\partial x_i} - \frac{2}{3}\frac{\partial \tilde{u}_l}{\partial x_l}\delta_{ij}\right) - \frac{2}{3}\bar{\rho}\tilde{k}\delta_{ij} \tag{9}$$

which accounts for the additional production caused by large density fluctuations. The averaged velocity fluctuation in Eqs. (7) and (8) is exactly given (Vallet et al., 2001) by

$$\bar{u_i'} = \bar{\rho}\widetilde{u_i'Y'}\left(\frac{1}{\rho_l} - \frac{1}{\rho_g}\right) \tag{10}$$

The solution of the above equations fully characterizes the large-scale bulk motion of the flow. Several other options exist for obtaining closure in the above system of equations [see, for example, the discussion in Demoulin et al. (2007) and Trask et al. (2012)].

The small-scale atomization is modeled by solving a transport equation for the evolution of the density of interphase surface area Σ, originally proposed by Vallet and Borghi (1999). The evolution equation is given by

$$\frac{\partial \overline{\Sigma}}{\partial t} + \frac{\partial \tilde{u}_j\overline{\Sigma}}{\partial x_j} = \frac{\partial}{\partial x_j}\left(D_\Sigma\frac{\partial \overline{\Sigma}}{\partial x_j}\right) + (A + a)\,\overline{\Sigma} - V_s\overline{\Sigma}^2 - \bar{\dot{\Sigma}}_{vap} \tag{11}$$

where D_Σ is a suitable diffusion coefficient usually taken as the turbulent viscosity over a Schmidt number. The terms A and a are inverse time scales that define the rate at which surface area is produced. Specifically, the A term models the creation of surface area via the stretching of the interface by mean velocity gradients. Vallet and Borghi's original model takes this term to be proportional to the same time scale as that used in the production of kinetic energy in the traditional k-ε model (Vallet and Borghi, 1999).

$$A = \alpha_0\frac{\bar{\rho}\widetilde{u_i''u_j''}}{\bar{\rho}k}\frac{\partial \tilde{u}_i}{\partial x_j} \tag{12}$$

The a term accounts for small-scale interface area production. Here there are several possibilities, but if it is assumed that the dominant mechanism is related to the collision and breakup of droplets, the inverse of droplet collision time scale may be used (Vallet et al., 2001).

$$a_{coll} = \frac{\alpha_1}{(36\pi)^{2/9}}(l_t\Sigma)^{2/3}\left(\frac{\rho_l}{\bar{\rho}\tilde{Y}}\right)^{4/9}\frac{\varepsilon}{k} \tag{13}$$

The V_s term captures the effects of interface destruction by coalescence. It is determined by solving for the value of V_s that will provide an equilibrium value of Σ set by a predicted equilibrium droplet radius (r_{eq}).

$$\Sigma_{eq} = \frac{\tau_{prod}}{\tau_{destr}} = \frac{3\bar{\rho}\tilde{Y}}{\rho_l r_{eq}} \tag{14}$$

$$V_s = \frac{a_{coll}\rho_l r_{eq}}{3\bar{\rho}\tilde{Y}} \tag{15}$$

To fix the equilibrium radius, there are, again, several options but as in Vallet et al. (2001) it is given here by

$$r_{eq} = \alpha_2\frac{\sigma^{3/5}l_t^{2/5}}{k^{3/5}}\frac{(\bar{\rho}\tilde{Y})^{2/15}}{\rho_l^{11/15}} \tag{16}$$

Finally, the $\bar{\dot{\Sigma}}_{vap}$ term models the effects on interphase surface produced by evaporation. This term comes from Lebas et al. (2009).

$$\bar{\dot{\Sigma}}_{vap} = \frac{2}{3}\frac{\Sigma^2}{\bar{\rho}\tilde{Y}_l}\dot{m}_{l\to v} \tag{17}$$

The value of $\dot{m}_{l\to v}$ is related to the sink/source term for fuel liquid/vapor transport equations, $\tilde{\dot{Y}}_{vap}$, through the following equation.

$$\dot{m}_{l\to v} = \frac{\bar{\rho}\tilde{\dot{Y}}_{vap}}{\Sigma} \tag{18}$$

Together with the mass-averaged volume fraction, the interface surface-area density can be used to calculate the local Sauter mean diameter of the spray.

$$D_{32} = \frac{6\bar{\rho}\tilde{Y}}{\rho_l\bar{\Sigma}} \tag{19}$$

In order to account for spray evaporation, both an additional transport equation for vapor fuel mass fraction and also a procedure for calculating the source term from Eq. (1) have to be added to the model. The transport equation can be written in a similar way to the conservation of liquid fuel as:

$$\frac{\partial\bar{\rho}\tilde{Y}_v}{\partial t} + \frac{\partial\bar{\rho}\tilde{u}_i\tilde{Y}_v}{\partial x_i} = -\frac{\partial\bar{\rho}\widetilde{u'_i Y'_v}}{\partial x_i} + \bar{\rho}\tilde{\dot{Y}}_{vap} \tag{20}$$

A standard turbulent gradient law is used for closure in this transport equation. The sink/source terms for fuel liquid/vapor transport equations are calculated in terms of a rate needed to achieve local adiabatic saturation conditions. This can be written as

$$\dot{Y}_v = \frac{Y_{v,sat} - \tilde{Y}_v}{\tau_{evap}} \tag{21}$$

where $\tilde{Y}_v$ is the local vapor fuel mass fraction, $Y_{v,sat}$ is the value of vapor fuel mass fraction under adiabatic saturation conditions, and τ_{evap} is a relaxation time. As a first approach, the latter parameter has been set equal to the computational time step.

Finally, $Y_{v,sat}$ is calculated by means of a locally homogeneous flow (LHF) approach (Faeth, 1983). According to that, state relationships are applied to describe spray thermodynamic conditions under the assumption of local thermodynamic equilibrium. The enthalpy balance for the mixture is expressed in terms of an adiabatic mixing process:

$$\begin{aligned} h\left(T\right) = Z \cdot h_f\left(T_0\right) + \left(1 - Z\right) \cdot h_a\left(T_a\right) = Y \cdot h_{f,l}\left(T\right) + Y_v \cdot h_{f,v}\left(T\right) \\ + \left(1 - Y - Y_v\right) \cdot h_a\left(T\right) \end{aligned} \tag{22}$$

where $Z = Y + Y_v$ is the mixture fraction. Together with the thermodynamic equilibrium assumption, local temperature and composition can be derived (Pastor et al., 2008), from which $Y_{v,sat}$ will be fed into the vaporization term of the transport equation.

2.2 Numerical Implementation

The model was implemented using the OpenFOAM (Weller et al., 1998) library. The advantages of this library are that polyhedral mesh and parallelism are intrinsically supported. The implementation of the governing equations largely follows the description in Trask et al. (2012). The present work, however, includes one notable numerical improvement, which maintains the mathematical consistency of the numerical solution. The issue concerns the relationship between density and mass fraction.

In Trask et al. (2012), the continuity equation was solved at the beginning of each time step in order to facilitate the computation of temporal derivatives such as those in Eqs. (1), (7), and (8), as well as the momentum equations. The computation of mass fraction transport by Eq. (1) then can represent the modeled turbulent dispersion of liquid mass. However, the combined solutions of Eqs. (1) and (2) create a constraint in order to maintain consistency with the definition of density, as given in Eq. (3). The implementation of Trask et al. (2012) did not guarantee that consistency would always be maintained between density and mass fraction.

The solution to this issue was to create a small penalty function in the pressure projection step. This penalty function is the last term in the pressure equation, Eq. (23), displayed below. The function relaxes the density calculated from the continuity equation

towards the value stipulated by Eq. (3). The constant multiplier, K_r, in this term represents the approximate number of time steps for relaxation to the correct density.

$$\nabla \cdot \phi^* - \nabla \cdot \left(\frac{1}{a_p} \nabla \bar{p} \right)_f = - \left(\frac{\bar{Y} \psi_l}{\rho_l} + \frac{1 - \bar{Y}}{\bar{p}} \right) \frac{D\bar{p}}{Dt} + \frac{1 - \bar{Y}}{T} \frac{DT}{Dt} - \left[\frac{1}{\rho_l} - \frac{1}{\rho_g} \right] \nabla \cdot \bar{\rho} \widetilde{u_i' Y'} - \frac{\rho_{eos} - \rho}{\delta_t K_r \rho} + \bar{\rho} \dot{\tilde{Y}}_{vap} \tag{23}$$

This pressure projection is inspired by the pressure/velocity coupling of the PISO method (Ferziger and Peric, 2002). The left side of Eq. (23) includes the standard terms in a pressure projection step, with ϕ representing the flux at cell faces and a_p representing the diagonal coefficient from the momentum equation. In Eq. (23) the symbol ϕ^* denotes the flux without the pressure gradient. The right-side terms are the compressibility, enthalpy, two-phase mixing, and numerical relaxation contributions, respectively. The term $\rho_{eos} - \rho$ represents the numerical discrepancy and δ_t is the time step. This approach successfully maintained consistency without iterative solutions of the continuity and mass transfer equations.

3. EXPERIMENTAL DATA

The data for model evaluation were obtained from two different databases of specific test rigs for Diesel spray characterization. Both of them were generated by single-hole axisymmetric nozzles, using a high-pressure common rail system.

For nonvaporizing sprays, data from Payri et al. (2008, 2011) have been used. In those experiments, the sprays were injected into a quiescent vessel where back pressure is modified at constant room temperature, so that ambient densities from 10 to 40 kg/m^3 are obtained in a nonvaporizing environment. Injection pressures ranged between 30 and 130 MPa.

The nozzle geometry characteristics are summarized in Table 1, where D, L, and r denote nozzle orifice outlet diameter, length, and inlet radius, respectively. The nozzle convergence is described by the k-factor, as defined in Macián et al. (2003)

This convergent nozzle was hydro-eroded in order to round the edges of the orifice inlet. Both geometric characteristics are aimed to prevent cavitation, as demonstrated by the hydraulic characterization presented in Payri et al. (2012).

Spray macroscopic characteristics, namely penetration and cone angle, have been obtained by high-speed imaging. A detailed description of the experimental setup and

TABLE 1: Nozzle geometric characteristics for nonvaporizing tests

***D* (mm)**	***L/D***	***r/D***	***k*-factor**
0.112	8.93	0.30	2.1

image acquisition methodology can be found in Payri et al. (2011). Regarding image processing, a validated methodology for segmentation (Pastor et al., 2007) was used. An additional source of spray data are the droplet size and velocity measurements from Payri et al. (2008), performed at different axial sections located from 25 to 50 mm to the orifice. As described in Araneo et al. (2006), a specific optimization of the PDPA system has been performed in order to improve measurements at those conditions.

In order to evaluate the model under vaporizing conditions, the ECN-Spray A database (ECN, 2012) has been used. The "Spray A" condition consists of a free Diesel spray injected into a quiescent environment, where well-defined boundary conditions and experimental data are available for model validation purposes. The nominal condition for Spray A corresponds to 150 MPa injection pressure, 900 K ambient temperature, and 22.8 kg/m^3 as ambient density. Parametric variations are performed based on this reference case.

In addition to standard spray characterization parameters such as liquid and vapor tip penetration (Bardi et al., 2012), a remarkable feature is that local air/fuel ratio measurements have been performed by means of a Rayleigh-scattering technique (Pickett et al., 2011). In the same way as for nonvaporizing sprays, convergent nozzles are used for Spray A. Detailed internal nozzle geometric characterization has been performed for the injectors employed in these experiments, where the main characteristics are presented in Table 2.

4. RESULTS AND DISCUSSION

4.1 Model set-up

In order to simulate the Diesel sprays, a 2D axisymmetric computational domain with 80 $\times$ 25 mm extent in the axial and radial spray directions is considered. The mesh is structured with nonuniform grid resolution. There are 10 cells along the orifice diameter, keeping an aspect ratio close to 1 in the near nozzle region, as depicted in Fig. 1. A mesh size convergence study was performed in order to achieve grid-independent results. The grid used in the calculations is comprised of 450 $\times$ 80 cells, with a cell expansion ratio of 1.01 and 1.06 in the axial and radial directions, respectively.

A Gamma NVD scheme is used for discretization of divergence terms and a first order Euler scheme is applied for time derivative terms. The inlet velocity boundary condition is obtained from mass flow rate and momentum flux measurements, applying

TABLE 2: Nozzle geometric characteristics for vaporizing sprays (ECN injectors)

Injector serial no.	*D* (mm)	*L/D*	*r/D*	*k*-factor
210675	0.0894	11.5	0.23	2.7
210677	0.0837	12.3	0.18	3.2

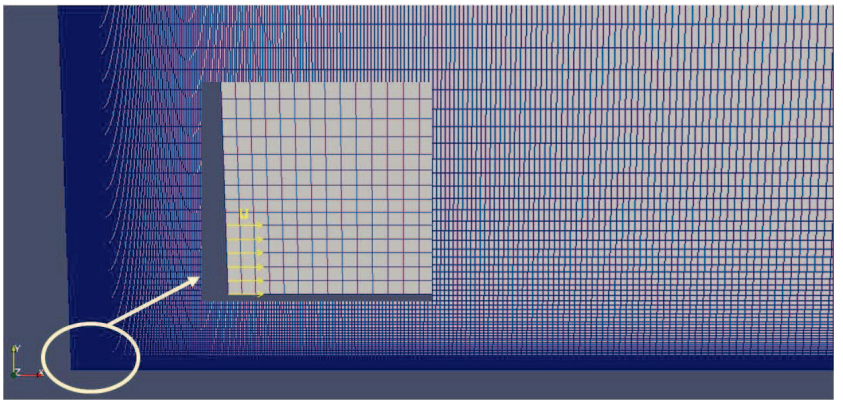

FIG. 1: Computational grid: The inset shows the mesh near the nozzle exit.

a constant radial profile of axial velocity and density at the nozzle outlet. The turbulent intensity was set to 5% and the length scale to 10% of the nozzle diameter.

One of the main assumptions of the Σ-Y model is the calculation of spray dispersion from a variable density turbulent mixing flow. Thus, it is expected that turbulence modeling will have a strong effect on spray predictions. As previously described, a modified form of the k-ε model accounting for density variations is employed. Due to the well known round jet spreading overprediction of k-ϵ type models (Pope, 1978), two different values for $C_{1\epsilon}$ constant were evaluated: the standard (1.44) and a corrected one (1.60). Pope (1978) has previously suggested that the latter value should be used for round jets. Though more refined expressions have been formulated for liquid turbulent flux closure (Beau et al., 2005), a gradient closure with Sc_t = 0.9 is used for this term. Results presented by Lebas et al. (2009) and Lebas (2007) indicate that this formulation could be sufficiently accurate for high-speed Diesel spray modeling.

Initial simulations under nonvaporizing conditions were run for the 80 MPa injection pressure and 40 kg/m^3 ambient density conditions, in order to evaluate the accuracy of the modeling approach. Results shown in Fig. 2 indicate that good agreement of spray penetration, and also centerline velocity, are obtained when using the corrected $C_{1\epsilon}$ value. A noticeable underestimation is obtained when using the standard value. Moreover, the measured radial profiles of axial velocity can only be captured with the corrected $C_{1\epsilon}$, as depicted in Fig. 3. It is also observed from this figure that self-similar velocities profiles are obtained for both measurements and calculations at different axial locations. These results indicate that both spray penetration and dispersion, which are related parameters, can be accurately predicted with the proposed model setup. It is also noticeable that spray penetration is well predicted at initial stages but also far downstream of the primary atomization region. The agreement between the model bulk velocity and the liquid measured one indicates very low slip between phases, at least for those conditions and measurement locations. This dynamic equilibrium also supports the

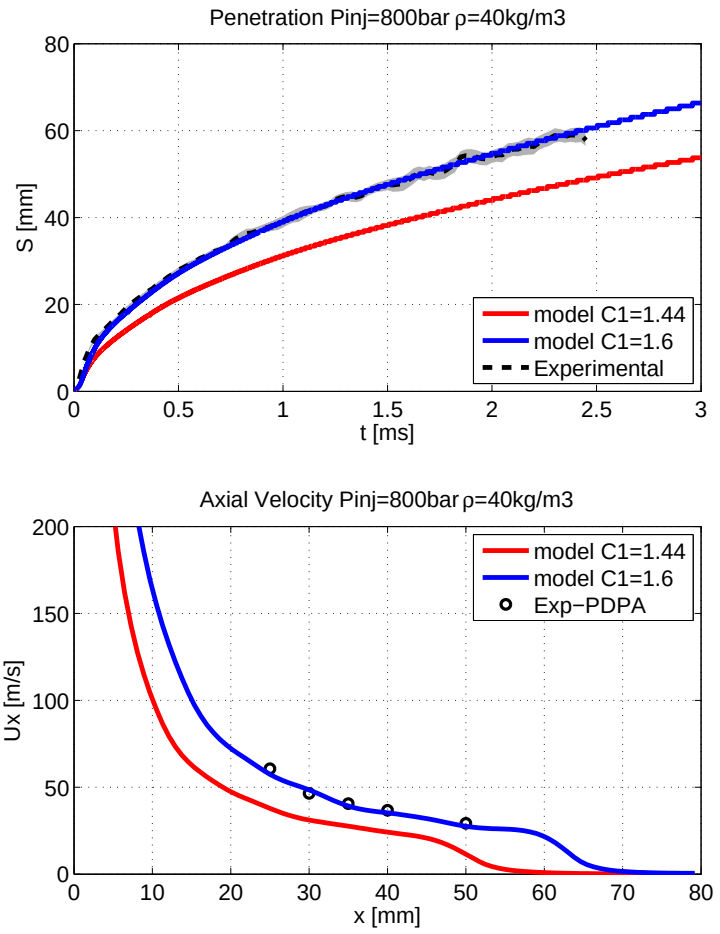

FIG. 2: Spray tip penetration and centerline axial velocity.

use of a gradient closure for liquid turbulent flux, which provides very low slip velocities (Beau et al., 2005).

The next step for model setup, after validation of large-scale flow, is focused on the small-scale atomization characteristics given by the interface surface density (Σ) and the droplet size derived from this variable. In these calculations, constants for both source and sink terms in the Σ equation correspond to the values proposed in Demoulin et al. (2007), but the α_2 model constant is set to 2.5 in order to provide fair agreement with measured SMD results.

Figure 4 shows the predicted spray SMD contours, where smaller drop sizes appear of just downstream the liquid core and after that SMD increases progressively with axial distance. Such droplet size increase, which has been observed in nonvaporizing experiments both in the present and also in previous works (Araneo and Tropea, 2000; Baik

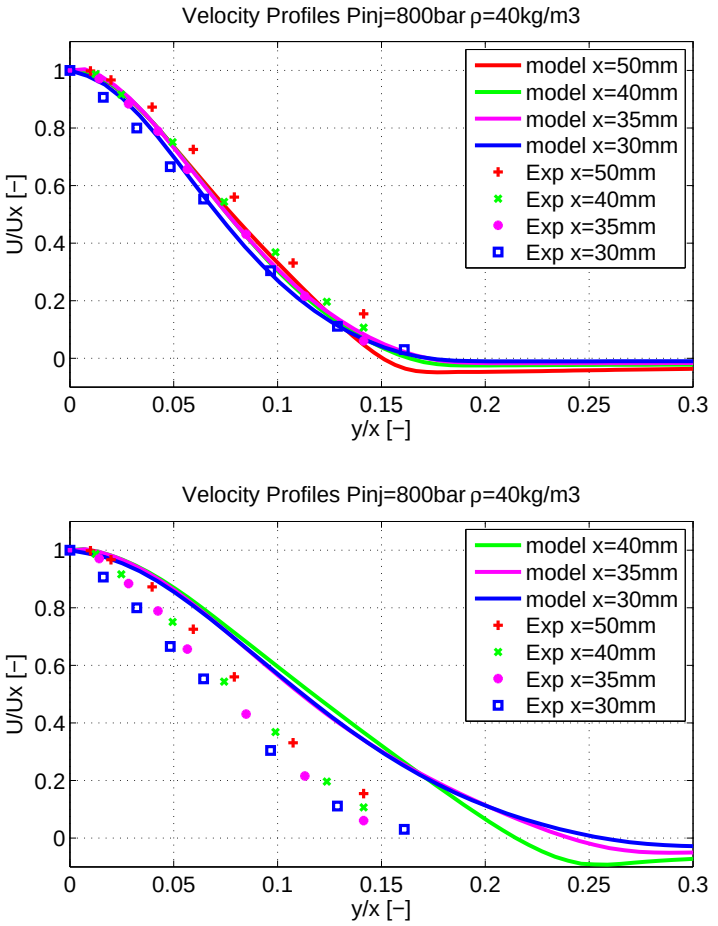

FIG. 3: Measured and predicted normalized radial profiles of axial velocity with CFD model using $C_{1\epsilon}$ = 1.6 (top) and $C_{1\epsilon}$ = 1.44 (bottom).

et al., 2003), is usually attributed to droplet coalescence. The behavior is also obtained in calculations due to the predominance of surface density sink terms on Eq. (11), probably caused by the increased equilibrium radius r_{eq} with lower kinetic turbulent energy k. However, the measured SMD axial increase is smaller than in computations, as depicted in Fig. 5, especially for near-axis locations.

4.2 Model Evaluation: Nonvaporizing Sprays

The model setup defined in the previous section was further assessed by simulating a series of experiments with different ambient and injection conditions. The range of validity of the model was evaluated by running cases with lower ambient density (25 and 10 kg/m^3) and increased (130 MPa) and decreased (30 MPa) injection pressures. As

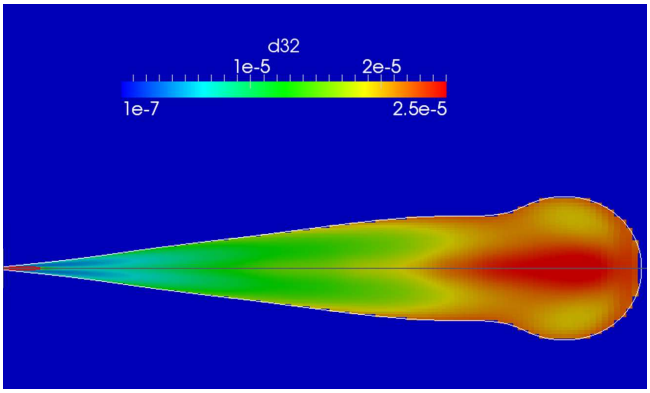

FIG. 4: Calculated SMD contours: White iso-line corresponds to $\overline{Y}$ = 1e-3.

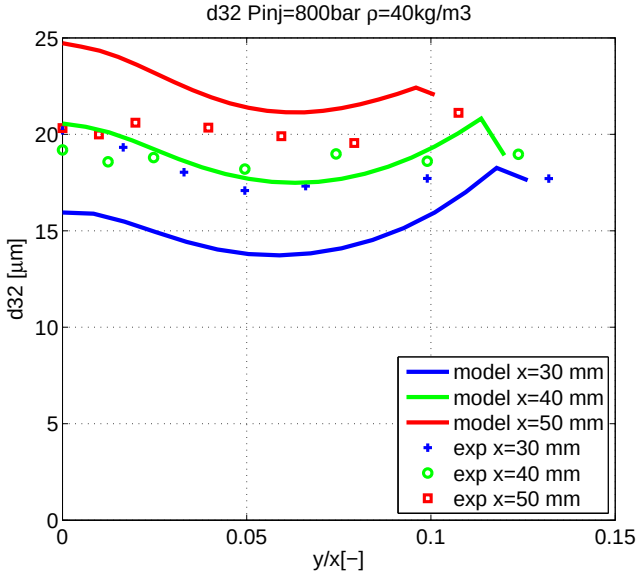

FIG. 5: Measured and predicted SMD profiles.

shown in Figs. 6–8, the accuracy of spray penetration predictions for high and intermediate ambient densities are similar, though some differences in centerline velocity results can be observed for ρ_a = 25 kg/m^3 conditions. Spray penetration is under-predicted for the lower ambient density, and also centerline velocities are lower than PDPA measurements. Velocity radial profiles from Fig. 9 show reduced spray dispersion as ambient density decreases, but the very narrow profiles for the lowest-density case cannot be captured by the model. All these results hint at the fact that spray dispersion is overpredicted when ambient density decreases.

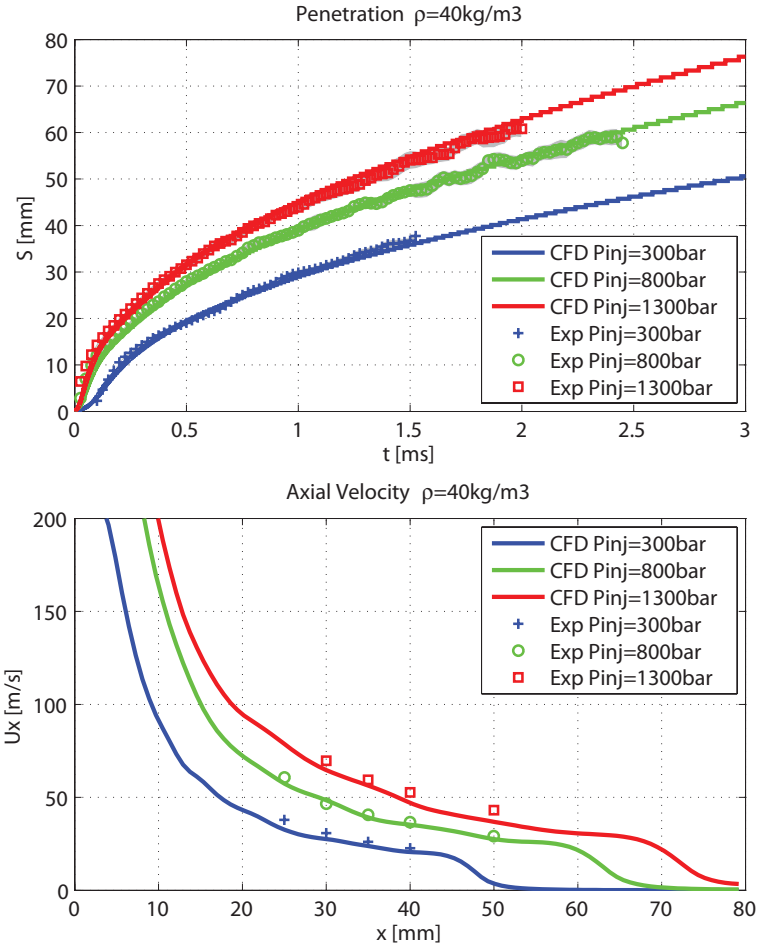

FIG. 6: Spray penetration (top) and centerline axial velocity (bottom) ρ_a = 40 kg/m^3.

Higher injection pressure does not modify the accuracy of spray characteristics predictions, and even good agreement on tip penetration is obtained for the lowest ambient density condition. Fair predictions are still found for P_{inj} = 300 bar and ambient densities of 40 and 25 kg/m^3. Major discrepancies have been obtained for the lowest density and injection pressure condition. In this case both Reynolds number and ambient-to-fuel density ratio are decreased, so this may have an effect on the spray atomization regime (Reitz and Bracco, 1986) and compromise the validity of the model assumptions. The slip between phases in these conditions is more significant and then the addition of a Lagrangian tracking for sparse spray regimes (Blokkeel et al., 2003) or a detailed model for the diffusion flux term closure, such as suggested in Beau et al. (2005), could provide better predictions.

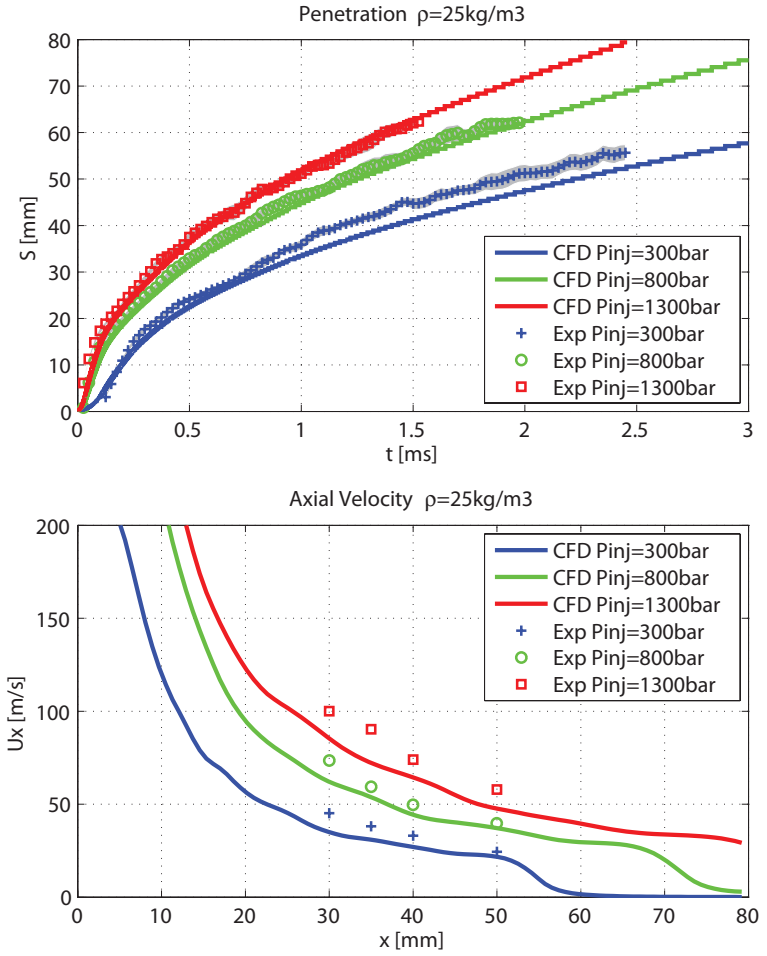

FIG. 7: Spray penetration (top) and centerline axial velocity (bottom) ρ_a = 25 kg/m^3.

Figure 10 shows the predicted and measured SMD data at the same section as the velocity profiles from Fig. 9. It is shown that SMD decreases with lower ambient density, probably due to lower coalescence after the primary atomization region Reitz (1987). This trend is captured by the model, but the effect is overestimated. Concerning injection pressure effects, SMD increases for lower injection pressures, as expected, but also here the trend is overestimated compared to experimental data.

4.3 Model Evaluation: Vaporizing Sprays

Vaporizing sprays are simulated using the same computational setup as defined in Section 4.1 for nonvaporizing cases. Spray A specifications were selected as the base case

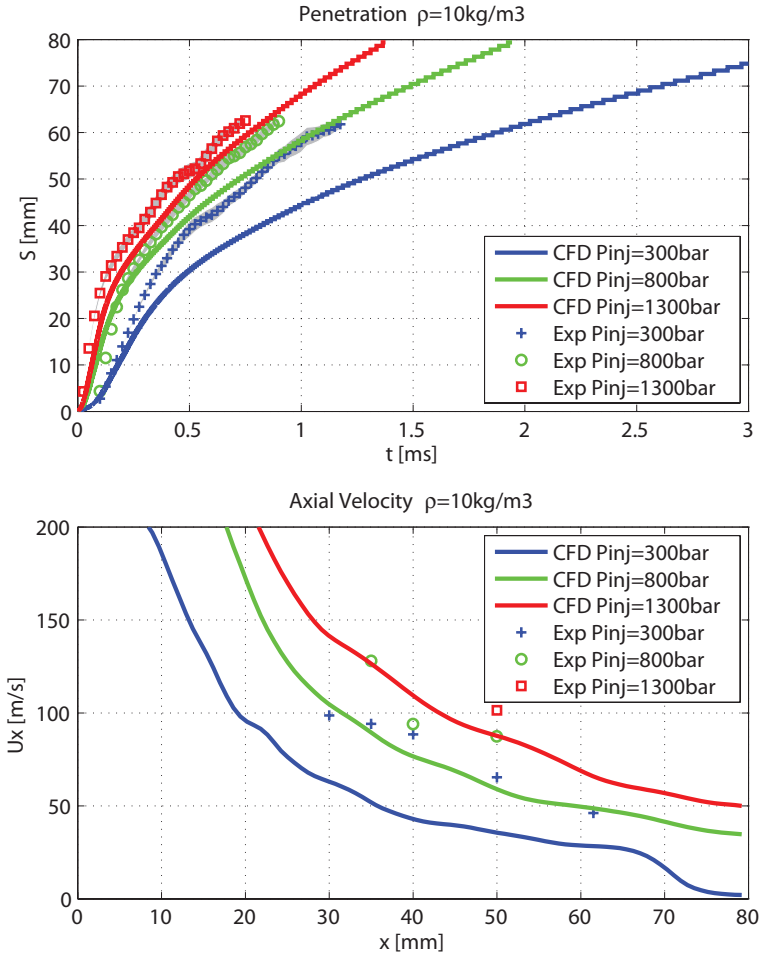

FIG. 8: Spray penetration (top) and centerline axial velocity (bottom) ρ_a = 10 kg/m^3.

simulation to evaluate model predictions. Results shown in Fig. 11 depict good agreement for both liquid and vapor penetration. In both cases, predictions are within the experimental error interval of measured values. The accuracy in maximum liquid length predictions confirms that the evaporation process under Spray A conditions is mainly mixing-controlled.

Predicted vs measured mixture fraction profiles are also shown in Figs. 12 and 13. Measurements are only available farther downstream of maximum liquid length distance, where the spray is fully in gas phase. Predicted values on the axis always fall within the experimental error interval, except below 22 mm, where the measuring uncertainty is also larger. Regarding radial distribution of mixture fraction, the shape of the normalized profiles is also adequately predicted by the model, as shown in Fig. 13. There is a slight

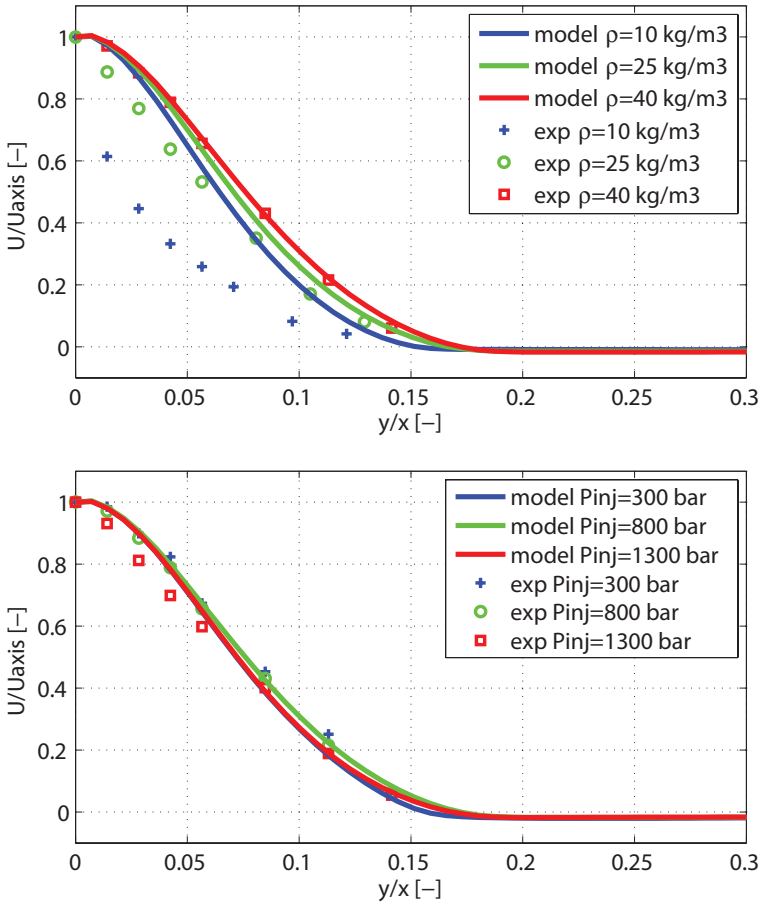

FIG. 9: Axial velocity radial profiles for P_{inj} = 800 bar (top) and ρ_a = 40 kg/m^3 (bottom) at x = 35 mm.

bias towards narrower radial profiles in the calculations, which should indicate less radial dispersion and hence slightly lower entrainment. This is also coherent with the fact that the on-axis mixture fraction is always in the upper part of the experimental error interval, and the same applies to spray tip penetration trends. However, the overall agreement is remarkable.

Parametric studies with different injection conditions, as well as with different ambient density and temperature, were also performed. Spray vapor penetration and liquid length predictions have been summarized in Figs. 14–16. Trends of decreasing vapor penetration with decreasing injection pressure and increasing penetration when decreasing ambient density are captured by the model. In general, good agreement between calculations and experiments is obtained, with most of the predicted results within experimental uncertainties. Effects of ambient density and temperature on quasi-steady

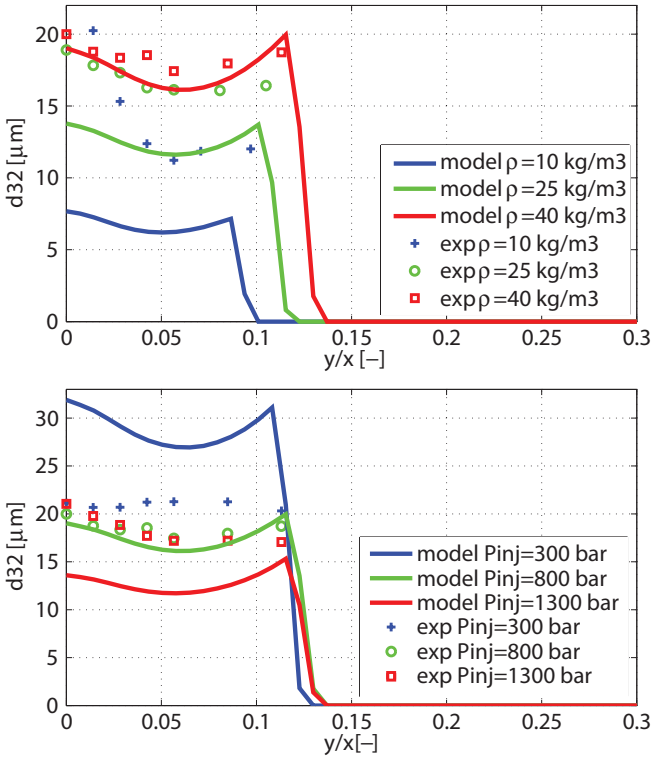

FIG. 10: SMD radial profiles for P_{inj} = 800 bar (top) and ρ_a = 40 kg/m^3 (bottom) at x = 35 mm.

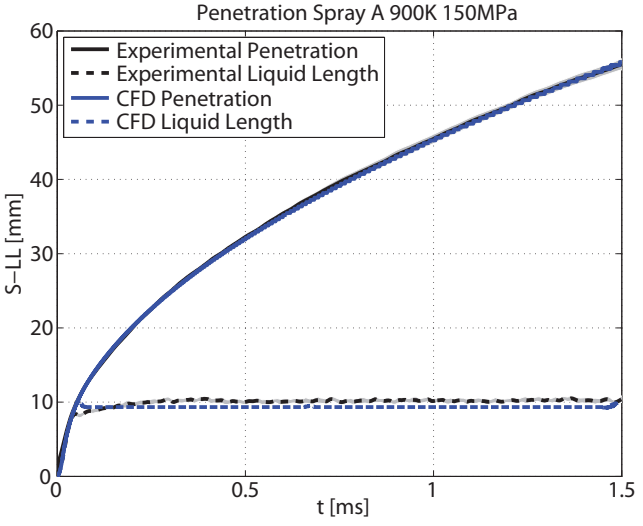

FIG. 11: Computed and measured liquid and vapor penetration: Injector 210677, P_{inj} = 150 MPa, T_a = 900 K, and ρ_a = 22.8 kg/m^3.

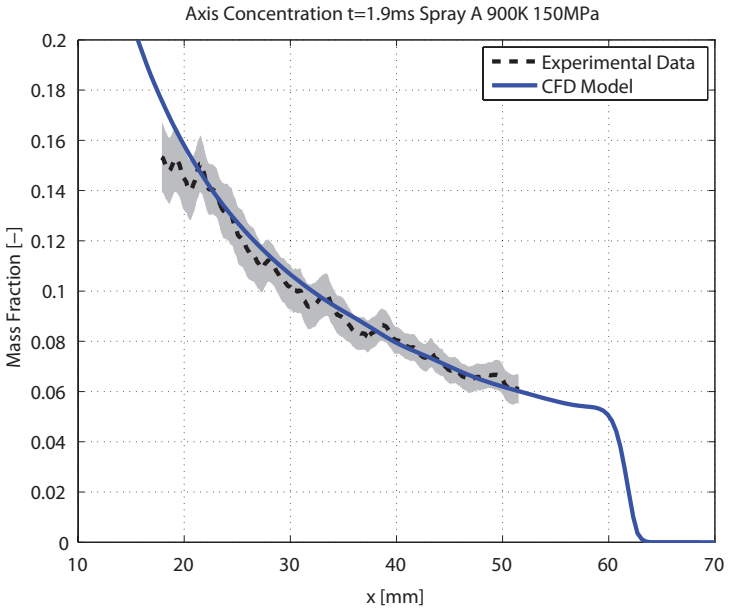

FIG. 12: Computed and measured centerline mixture fraction: Injector 210677, P_{inj} = 150 MPa, T_a = 900 K, and ρ_a = 22.8 kg/m^3.

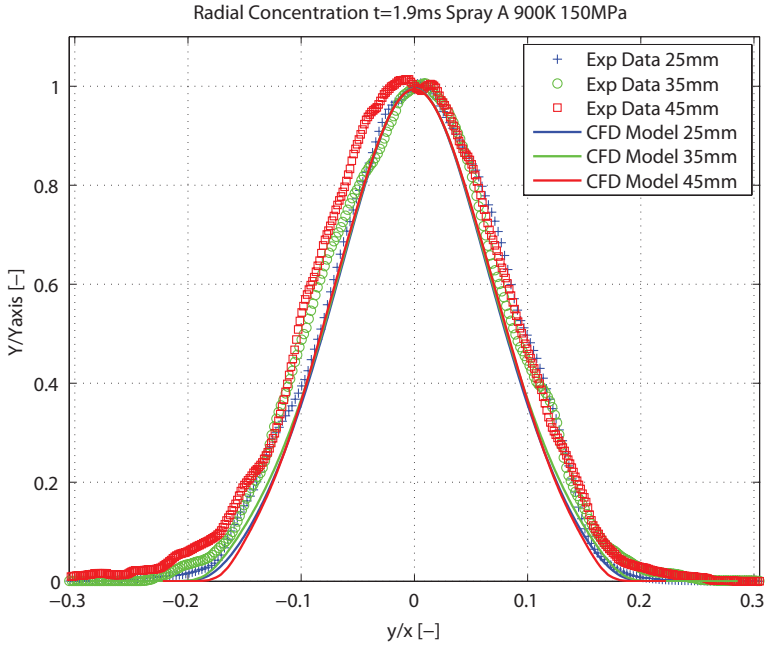

FIG. 13: Computed and measured mixture fraction radial profiles: Injector 210677, P_{inj} = 150 MPa, T_a = 900 K, and ρ_a = 22.8 kg/m^3.

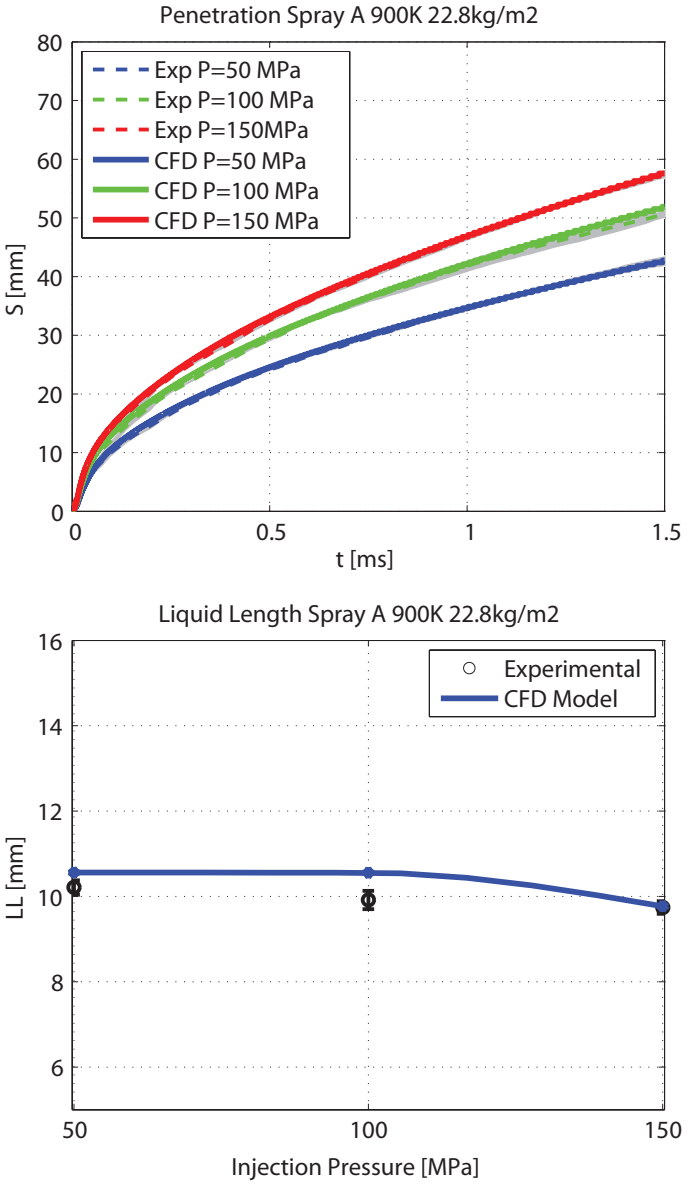

FIG. 14: Computed and measured vapor and liquid penetration for different injection pressures: Injector 210675, T_a = 900 K, and ρ_a = 22.8 kg/m^3.

values of liquid length are also well predicted. Departures tend to be noticeable at the lowest density conditions, which could be expected from the nonvaporizing spray results. This agreement also confirms that evaporation model hypotheses are valid over a wide range of operating conditions of current diesel engines.

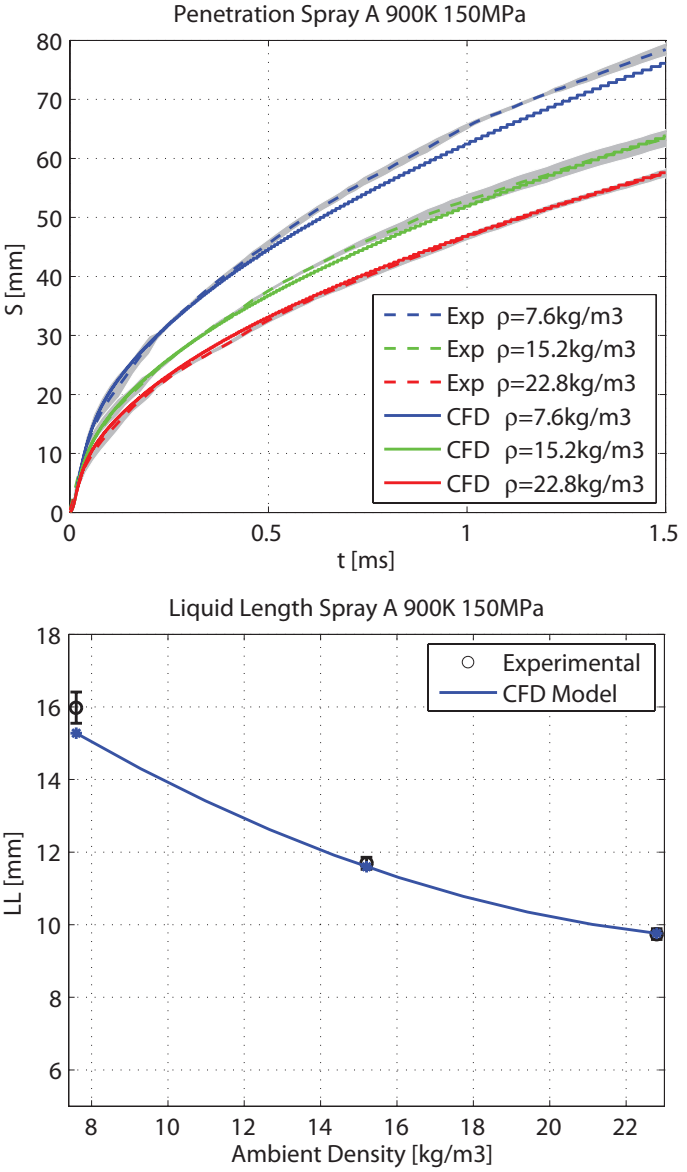

FIG. 15: Computed and measured vapor penetration and liquid length for different conditions of ambient density: Injector 210675, P_{inj} = 150 MPa, and T_a = 900 K.

5. SUMMARY AND CONCLUSIONS

A fully compressible implementation of the Σ-Y model has been applied to the study of direct injection Diesel sprays. As opposed to Lagrangian-Eulerian DDM modeling, the present approach makes it possible to compute two-phase flows using a highly refined

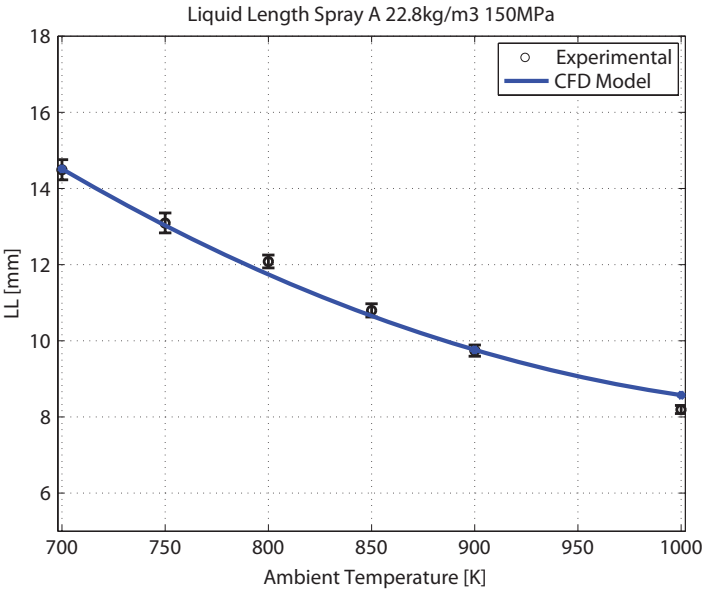

FIG. 16: Computed and measured liquid length for different conditions of ambient temperature: Injector 210675, P_{inj} = 150 MPa, and ρ_a = 22.8 kg/m^3.

mesh without going into numerical instabilities. Calculations have been validated against spray test rig experiments for both nonvaporizing and vaporizing sprays under different operating conditions. Spray tip penetration and liquid-phase lengths, as well as spatial distribution of axial velocity, droplet size, and fuel mass fraction have been used for validation.

Model setup has been performed by modifying the $C_{1\epsilon}$ constant of the k-ϵ turbulence model, as previously suggested for round jets, as well as the α_2 constant in the Σ equation. In both cases, selected values have been kept constant for all calculations.

For nonvaporizing sprays, predicted spray tip penetration and velocity fields were in very good agreement with the experimental data under medium and high ambient gas density conditions. When the ambient gas density was low, agreement was not as good, suggesting that under these conditions interfacial dynamics become more significant. Under such conditions, transition to a Lagrangian formulation in the sparse region of the spray would be more appropriate. The model suggested by Beau et al. (2005) may also improve the predictions in such low ambient density conditions. On the other hand, SMD predictions were only qualitatively correct. Although parametric trends were correct, the model was far more sensitive than experiments towards changes in operating conditions.

For vaporizing sprays, predicted spray tip penetration, fuel mass fraction field, and quasi-steady liquid lengths were also in agreement with experimental data. In this case, differences at lower density were not as noticeable as in the nonvaporizing case, due to the inherent transition to a single-phase flow.

The overall utility of the Σ-Y modeling approach is confirmed by the validation studies. The model is applicable to ambient gas density conditions that are normally present in Diesel engines, but would be less accurate for very early injection conditions, such as those found in highly premixed combustion strategies, due to the lower ambient density. The model is not yet capable of predicting drop sizes over the range of conditions studied. However, under such conditions spray penetration, dispersion, and vaporization processes are mainly mixing-controlled, and thus droplet-related phenomena are not the governing parameters. This view is confirmed by the ability to model vaporization accurately without having precise SMD predictions.

ACKNOWLEDGMENTS

This work was partially funded by the Spanish Ministry of Education and Science in the frame of the ENE2010-18542 project. The authors acknowledge support from the Army Research Office under grant no. W911NF-08-1-0171.

REFERENCES

Abraham, J., What is adequate resolution in the numerical computations of transient jets?, *SAE Trans. J. Engines*, vol. **106**, pp. 141–151, 1997.

Abraham, J. and Picket, L., Computed and measured fuel vapor distribution in a diesel spray, *Atomization Sprays*, vol. **20**, pp. 241–250, 2010.

Araneo, L., Soare, V., Payri, R., and Shakal, J., Setting up a PDPA system for measurements in a diesel spray, *J. Phys.: Conf. Ser.*, vol. **45**, pp. 85–93, 2006.

Araneo, L. and Tropea, C., Improving phase doppler measurements in a diesel spray, *SAE Technical Paper*, 2000-01-2047, 2000.

Baik, S., Blanchard, J., and Corradini, M., Development of micro-diesel injector nozzles via MEMS technology and effects on spray characteristics, *Atomization Sprays*, vol. **13**, pp. 443–474, 2003.

Bardi, M., Payri, R., Malbec, L., Brunneaux, G., Pickett, L., Manin, J., Bazyn, T., and Genzale, C., Engine combustion network: Comparison of spray development, vaporization and combustion in different combustion vessels, *Atomization Sprays*, vol. **22**, pp. 807–842, 2012.

Beau, P., Funk, M., Lebas, R., and Demoulin, F., Applying quasi-multiphase model to simulate atomization processes in diesel engines: Modeling of the slip velocity, *SAE Technical Paper*, 2005-01-0220, 2005.

Blokkeel, G., Barbeau, B., and Borghi, R., A 3D Eulerian model to improve the primary breakup of atomizing jet, *SAE Technical Paper*, 2003-01-005, 2003.

Demoulin, F., Beau, P., Blokkeel, G., Mura, A., and Borghi, R., A new model for turbulent flows with large density fluctuations: Application to liquid atomization, *Atomization Sprays*, vol. **17**, pp. 315–345, 2007.

Desportes, A., Zellat, M., Desoutter, G., Liang, Y., and Ravet, F., Application of the Eulerian-

Lagrangian spray atomization (ELSA) model for the diesel injection simulation, *Proc. of THIESEL 2010 Conference on Thermo- and Fluid Dynamic Process in Diesel Engines*, 2010.

Dukowicz, J., A particle fluid numerical model for liquid sprays, *J. Comput. Phys.*, vol. **2**, pp. 111–566, 1980.

ECN, 2012. http://www.sandia.gov/ECN/

Faeth, G., Evaporation and combustion of sprays, *Prog. Energy Combust. Sci.*, vol. **9**, pp. 1–76, 1983.

Ferziger, J. and Peric, M., *Computational Methods for Fluid Dynamics*, Springer, Berlin, pp. 176–178, 2002.

Gorokhovski, M. and Herrmann, M., Modeling primary atomization, *Ann. Rev. Fluid Mech.*, vol. **40**, pp. 343–366, 2008.

Iyer, V. and Abraham, J., Penetration and dispersion of transient gas jets and sprays, *Combust. Sci. Technol.*, vol. **130**, pp. 315–334, 1997.

Lebas, R., *Modélisation Eulerienne de l'Atomisation Haute Pression Influences sur la Vaporisation et la Combustion Induite*, PhD Thesis, University of Rouen, 2007.

Lebas, R., Blokkeel, G., Beau, P., and Demoulin, F., Coupling vaporization model with the Eulerian-Lagrangian spray atomization (ELSA) model in diesel engine conditions, *SAE Technical Paper*, 2003-01-005, 2005.

Lebas, R., Menard, T., Beau, P., Berlemont, A., and Demoulin, F., Numerical simulation of primary break-up and atomization: DNS and modeling study, *Int. Jo. Multiphase Flow*, vol. **35**, pp. 247–260, 2009.

Macián, V., Bermúdez, V., Payri, R., and Gimeno, J., New technique for determination of internal geometry of a diesel nozzles with the use of silicone methodology, *Exp. Tech.*, vol. **37**, pp. 39–43, 2003.

Ning, W., Reitz, R., Diwakar, R., and Lippert, A., An Eulerian-Lagrangian spray and atomization model with improved turbulence modeling, *Atomization Sprays*, vol. **19**, pp. 727–739, 2009.

Pastor, J., Arregle, J., Garcia, J., and Zapata, L., Segmentation of diesel spray images with log-likelihood ratio test algorithm for non-Gaussian distributions, *Appl. Opt.*, vol. **19**, pp. 888–899, 2007.

Pastor, J., López, J., García, J., and Pastor, J., A 1-D model for the description of mixing-controlled inert diesel sprays, *Fuel*, vol. **87**, pp. 2871–2885, 2008.

Payri, R., Tormos, B., Salvador, F., and Araneo, L., Spray droplet velocity characterization for convergent nozzles with three different diameters, *Fuel*, vol. **87**, pp. 3176–3182, 2008.

Payri, R., Salvador, F., Gimeno, J., and Novella, R., Flow regime effects on non-cavitating injection nozzles over spray behavior, *Int. J. Heat Fluid Flow*, vol. **32**, pp. 273–284, 2011.

Payri, R., Salvador, F., Gimeno, J., and Garcia, A., Flow regime effects over non-cavitating diesel injection nozzles, *Proc. Inst. IMechE, Part D*, vol. **226**, pp. 133–144, 2012.

Pickett, L., Manin, J., Genzale, C., Siebers, D., Musculus, M., and Idicheria, C., Relationship between diesel fues spray vapor penetration/dispersion and local fuel mixture fraction, *SAE Int. J. Engines*, vol. **4**, pp. 764–799, 2011.

Pope, S., An explanation of the turbulent round-jet/plane-jet anomaly, *AIAA*, vol. **16**, pp. 279–

281, 1978.

Reitz, R., Modeling atomization processes in high-pressure vaporizing sprays, *Atomization Spray Tech.*, vol. **3**, pp. 309–337, 1987.

Reitz, R. and Bracco, F., *The Encyclopedia of Fluid Mechanics*, Gulf Publishing, Houston, TX, 1986.

Schmidt, D. P. and Corradini, M. L., The internal flow of diesel fuel injector nozzles: A review, *J. Engine Res.*, vol. **2**, no. 1, pp. 1–22, 2001.

Siebers, D., Liquid-phase fuel penetration in diesel sprays, *Trans. SAE*, vol. **107**, pp. 1205–1227, 1998.

Siebers, D., Liquid-phase fuel penetration in diesel sprays based on mixing-limited vaporization, *Trans. SAE*, vol. **108**, pp. 703–728, 1999.

Siebers, D. L., Recent developments on diesel fuel jets under quiescent conditions, *Flow and Combustion in Reciprocating Engines*, Arcoumanis, C. and Kamimoto, T., Eds., Springer-Verlag, Berlin, pp. 257–308, 2008.

Som, S. and Aggarwal, S., Assessment of atomization models for diesel engine simulations, *Atomization Sprays*, vol. **19**, pp. 885–903, 2009.

Trask, N., Schmidt, D., Lightfoot, M., and Danczyk, S., Compressible modeling of the internal flow in a gas-centered swirl-coaxial fuel injector, *J. Propulsion Power*, vol. **28**, no. 4, pp. 685–693, 2012.

Vallet, A. and Borghi, R., Modélisation Eulerienne de l'atomisation d'un jet liquide, *C.R. Acad. Sci., Paris*, vol. **327**, pp. 1015–1020, 1999.

Vallet, A., Burluka, A., and Borghi, R., Development of a Eulerian model for the "atomization" of a liquid jet, *Atomization Sprays*, vol. **11**, pp. 619–642, 2001.

Weller, H., Tabor, G., Jasak, H., and Fureby, C., A tensorial approach to computational continuum mechanics using object-oriented techniques, *Comput. Phys.*, vol. **12**, pp. 620–631, 1998.